J. Membrane Biol. 181, 163–170 (2001)
DOI: 10.1007/s00232-001-0019-2

The Journal of
Membrane
Biology

Sodium Blocking Induced by a Point Mutation at the C-Terminal End of the Pore Helix of the KAT1 Channel

N. Uozumi[1], K. Yamada, S. Goshima[1], T. Ona[2], S. Oiki
Department of Physiology, Fukui Medical University, Yoshida-gun, Fukui 910-1193, Japan
[1]Nagoya University Bioscience Center, Nagoya University, Chikusa-ku, Nagoya 464-8601, Japan
[2]Forestry Research Institute, Oji Paper Co., Ltd., 24-9 Nobono-cho, Kameyama 519-0212, Japan

Received: 16 October 2000/Revised: 20 February 2001

Abstract. A plant hyperpolarization-activating K^+ channel, KAT1, is highly selective for K^+ over Na^+ and is little affected by external Na^+, which is crucial to take up K^+ effectively in a Na^+-containing environment. It has been shown that a mutation at the location (Thr256) preceding the selectivity signature sequence dramatically enhanced the sensitivity of the KAT1 channel to external Na^+. We report here electrophysiological experiments for the mechanism of action of external Na^+ on KAT1 channels. The Thr256 residue was substituted with either glutamine (Q) or glutamate (E). The wild-type channel was insensitive to external Na^+. However, the activity of both mutant channels was significantly depressed by Na^+ with apparent dissociation constants of 6.7 mM and 11.3 mM for T256Q and T256E, respectively. The instantaneous current-voltage relationships revealed distinct blocking mechanisms for these mutants. For T256Q a typical voltage-dependent fast blocking was shown. On the other hand, the blocking for the T256E mutant was voltage-independent at low Na^+ concentrations and became voltage-dependent at higher concentrations. At extreme hyperpolarization the blocking was relieved significantly. These data strongly suggest that the mutation at the end of the pore helix rearranged the selectivity filter and allows Na^+ to penetrate into the pore.

Key words: Open channel blocking — Electrophysiology — Selectivity — Channel structure — Hyperpolarization activating channel — Instantaneous current-voltage curves

Correspondence to: S. Oiki

Introduction

Intracellular Na^+ induces detrimental effects on growing plant cells (Kingsbury & Epstein, 1986), while it plays regulatory roles in some animal cells, such as myocardial cells (Kameyama et al., 1984). The dramatic contrast for the requirements of intracellular Na^+ ions between plant and animal cells suggests different functional roles for the ion transport systems. Among these, potassium channels in plant cells, in contrast to their counterparts in animal cells, carry inward K^+ flux through channels open at physiological membrane potential, which is hyperpolarized to the equilibrium potential for K^+ (Schroeder, Ward & Gassmann, 1994). Consequently, potassium channels in plant cells are subject to competition with external Na^+ for carrying inward K^+ flux. To prevent such interference by external Na^+ it is likely that plant potassium channels are equipped to exclude Na^+ from entering the pore. KAT1 isolated from an *Arabidopsis thaliana* cDNA library as a K^+ uptake system shows similar membrane topology to that of animal *Shaker*-type K^+ channels (Anderson et al., 1992; Uozumi et al., 1998; Hoshi, 1995; Schachtman et al., 1992). The signature sequence of the KAT1 channel is well conserved with those of *Shaker* K^+ channels. Many site-directed mutageneses have been introduced into the pore region of KAT1 to elucidate structure-function relationships (Uozumi et al., 1995; Moroni et al., 2000; Lacombe and Thibaud, 1998; Dryer et al., 1998; Ichida and Schroeder, 1996). Among the mutations introduced, Uozumi et al. (1995), using the yeast expression system, reported that the conversion of threonine 256 (Thr256), located at the middle of the P-region, in KAT1 channels imparted Na^+ sensitivity to the K^+ uptake ability. For the T256Q and T256E mutant KAT1 channels expressed in oocytes, an inhibition of the inward K^+ current by external Na^+ was clearly demonstrated.

Recent elucidation of the canonical structure of potassium channels (Doyle et al., 1998) provided a solid basis for interpreting functional data, such as those from electrophysiological experiments. Among other structural parts the selectivity filter should hold its architecture throughout the potassium channel gene family. Here, we focused on the mechanism of the Na^+ effect on the wild-type (WT) and mutant KAT1 channels through electrophysiological analyses. Based on the structural information, Na^+-sensitivity induced by the mutation would provide clues for the mechanism how the KAT1 channel could effectively exclude Na^+ from entering the pore in environments in which external Na^+ and K^+ may compete for travel through the pore.

Materials and Methods

Channel Expression

Complementary RNAs for wild type KAT1, T256Q and T256E channels were synthesized as described previously (Uozumi et al., 1995). Oocytes were removed surgically from *Xenopus laevis* toads and defolliculated by incubating with agitation for 1 hr in a solution containing collagenase (Type I, 1 mg/mg; Sigma, St. Louis, MO). Defolliculated oocytes were injected with cRNA and incubated at 19°C.

Electrophysiology

Two-electrode voltage-clamp experiments were performed using a Dagan CA1 amplifier (Dagan, Minneapolis, MN). The detailed descriptions of the electrophysiological experiments are as described in Sabirov et al. (1997). Oocytes were perfused with a solution containing (mM): 30 KCl, 80 NMDG, 5 HEPES, pH 7.4 with Tris. Recorded currents were filtered at 1 kHz (four-pole Bessel) and digitized at 5 kHz. pCLAMP was used for electrophysiological measurements and the fitting of current traces with the multi-exponential function. Microelectrode resistances were between 0.2 and 0.8 MΩ when filled with 3 M KCl. All experiments were performed at room temperature (25°C). For the solution of different Na^+ concentrations NMDG was used as an "inert" cation and the ionic strength was kept constant.

Data Analysis

The "steady-state" gating curves were obtained from the "tail" current recordings. The channel was activated by applying −150 mV for 500 msec and then stepped to various membrane potentials ranging from 0 to −200 mV. Deactivating or activating current traces were fitted by a triple-exponential function:

$$I(t) = A_1 \exp\left[-\frac{t}{\tau_1}\right] + A_2 \exp\left[-\frac{t}{\tau_2}\right] + A_3 \exp\left[-\frac{t}{\tau_3}\right] + C$$

where A's are amplitude components, τ's are time constants and C is a constant, time-independent component. The "steady-state" current level was attained from the DC components, C in the above equation, of the fitted parameters. Each steady-state current amplitude was divided by the instantaneous current amplitude of the corresponding membrane potential to get the normalized gating value.

To evaluate the gating properties of the channels, we considered that the channel exhibits transitions between two states (closed and open). The normalized gating properties were fitted with a single Boltzmann function according to:

$$G = \frac{1}{1 + \exp\left[\frac{V - V_{1/2}}{dV}\right]}$$

where $V_{1/2}$ is the half activation voltage and dV is the slope constant. The fitted curves were normalized for the abscissa by the fitted maximal values.

The data for the concentration-dependent current amplitudes were fitted to the equation:

$$\frac{I}{I_o} = \frac{K_d}{[Na^+]_o + K_d} + C$$

where I/I_o is the fractional current in the presence of external Na^+, K_d is the dissociation constant and C is a constant.

The permeability ratio was calculated from the shift of the reversal potential for different Na^+ concentrations using the Goldman-Hodgkin-Katz equation.

$$\frac{P_{Na}}{P_K} = \frac{[K^+]_o}{\Delta[Na^+]_o}\left(\exp\left[\frac{F\Delta V_{rev}}{RT}\right] - 1\right)$$

where ΔV_{rev} is the shift of the reversal potential upon changing the external Na^+ concentration (from 0 to 80 mM; the difference of the Na^+ concentration, $\Delta[Na^+]_o$, is 80 mM in this experiment).

The blocking was described by the Boltzmann function:

$$B = \frac{1 - C}{[Na^+]_o + \exp\left[\Delta G + \frac{F\delta V}{RT}\right]} + C$$

where ΔG is the free energy for the binding in RT unit, δ is the electrical distance, F is the Faraday constant, R is the gas constant and T is the absolute temperature. For the voltage-independent blocking the Michaelis-Menten equation was included for the blocking equation.

$$B = \left(\frac{1 - C}{1 + \frac{[Na^+]_o}{K_d}} + C\right) \frac{1 - [Na^+]_o \exp\left[-\Delta G_2 - \frac{F\delta_2 V}{RT}\right]}{1 + [Na^+]_o\left(\exp\left[-\Delta G_1 - \frac{F\delta_1 V}{RT}\right] + \exp\left[-\Delta G_2 - \frac{F\delta_2 V}{RT}\right]\right)}$$

Curve fittings were performed using Levenberg-Marquardt minimization procedures (Origin software; MicroCal Software, Inc.).

The number of observations was five unless noted otherwise.

Results

Activation of KAT1 Channels

Currents were recorded from *Xenopus* oocytes expressing either WT or mutant (T256Q and T256E) KAT1 channels under two-electrode voltage-clamped conditions. The membrane potential was stepped from a holding potential (V_h) of −40 mV to voltages ranging from −30 to −170 mV for 500 msec. Hyperpolarization-activated currents recorded in the external solution containing 30 mM K^+ are shown in Fig. 1*A* for WT and the

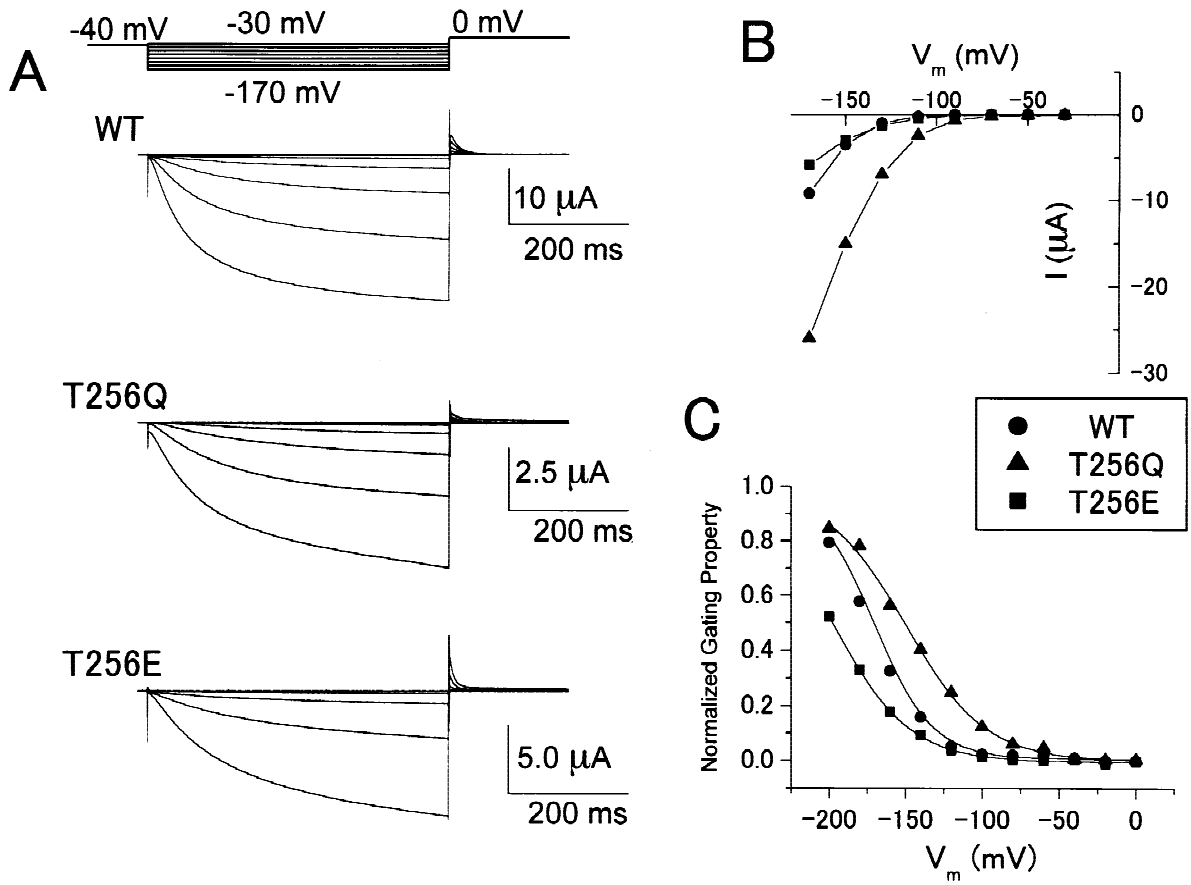

Fig. 1. Current recordings for the WT and mutant KAT1 channels. (A) Representative current traces for the WT channel and the mutant T256Q and T256E channels elicited by hyperpolarizing pulses under the two-electrode voltage-clamp condition. The kinetics of the activation differs significantly for the mutants. The tail currents are seen at 0 mV potential. The perfusing solution contains 30 mM K^+ and 80 mM $NMDG^+$. (*Inset*) The voltage command. Voltage pulses of 500 msec duration were applied from a holding potential of −40 mV and returned to 0 mV. The voltage ranges were from −30 to −170 mV with 20 mV steps. (B) The current-voltage curves at the end of the pulses. The current amplitudes measured at the end of the hyperpolarizing pulses are plotted as a function of the command voltages. ●: WT, ▲: T256Q, ■: T256E. (C) The "steady-state" gating curves. The normalized gating properties for the WT and the mutant channels are plotted as a function of the membrane potential. The current amplitude of the quasi-steady-state at each membrane potential was obtained from the tail current measurements (*see* the detailed description in Materials and Methods). The two-state Boltzmann function was used for the fitting. ●: WT, ▲: T256Q, ■: T256E. The $V_{1/2}$ was −175.0 ± 2.1 mV for the WT, −150.0 ± 3.1 mV for T256Q and −193.7 ± 4.1 mV for T256E. The slope constants were 20.1 ± 0.9 mV, 26.1 ± 1.7 mV and 23.8 ± 1.1 mV for WT, T256Q and T256E, respectively.

mutant channels. As the membrane potential was hyperpolarized the WT channel activated progressively with faster activation kinetics. Activation for the T256E mutant channel was slower, whereas activation of the T256Q mutant was slightly faster than that of the wild type. Deactivation kinetics observed from the tail current at 0 mV were faster for the T256Q and slower for the T256E channels. The current-voltage relationships at the end of the command potentials are shown in Fig. 1*B*. The voltage ranges of the activations were shifted by the mutations.

To investigate whether the effective gating charge might have been modified by the mutations, the steady-state gating properties were examined. In Fig. 1*C* the normalized gating curves are shown with the fitted curves using the two-state Boltzmann function (*see* Materials and Methods for details). In comparison to the wild-type channel ($V_{1/2}$ = −175.0 ± 2.1 mV), the T256Q mutation shifted the gating curve towards the depolarized direction ($V_{1/2}$ = −150.0 ± 3.1 mV), whereas the T256E mutation shifted it towards more hyperpolarized potential ($V_{1/2}$ = −193.7 ± 4.1 mV). For the T256Q mutant the steady-state gating curve was significantly deviated from zero at less hyperpolarized potentials, indicating that the channel is open even at a holding potential of −40 mV. The value of the voltage dependency (*dV*) for WT was 20.1 ± 0.9 mV and that for T256Q was 26.1 ± 1.7 mV. Thus, the gating charge was slightly altered by the T256Q mutation. The negative shift of the gating curve for T256E made the Boltzmann fit less re-

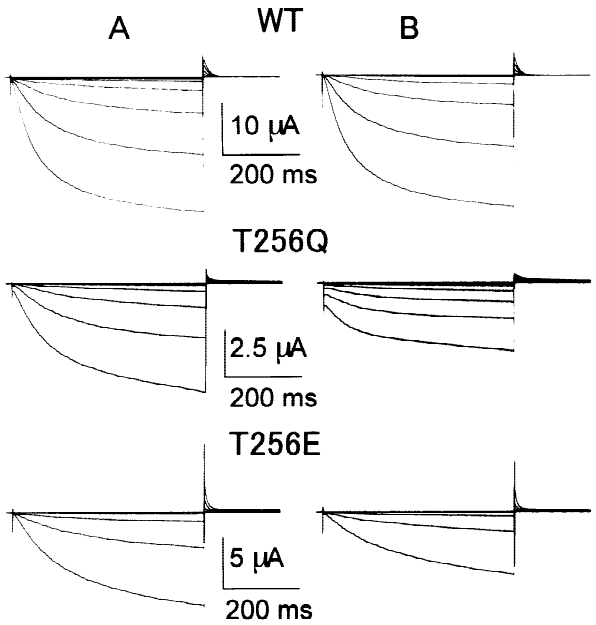

Fig. 2. Current traces with and without external Na^+. The current traces without (*A*) and with (*B*) 80 mM Na^+ in the external solution. The command potentials were the same as for Fig. 1*A*.

liable for the values of both $V_{1/2}$ (−193.7 ± 4.1 mV) and voltage dependency (23.8 ± 1.1 mV). In summary, the mutations on the P-region little affected the gating charges, while they shifted the activation voltages.

Current Inhibition by External Na^+

Uozumi et al. (1995) demonstrated that the mutation sensitized the channel to external Na^+. The WT channel was little affected by Na^+, while the current of both mutant channels was depressed as the external K^+ was replaced by Na^+. To investigate the mechanism of Na^+ inhibition, the external Na^+ concentration was increased up to 80 mM by replacing NMDG at a fixed concentration of 30 mM K^+. In Fig. 2 the current traces with (*B*) and without 80 mM Na^+ (*A*) are shown. Na^+ decreased the current in mutant channels. This inhibitory effect was reversible (*not shown*). Representative current-voltage curves measured at the end of the command potential for different Na^+ concentrations are shown in Fig. 3*A*. In Fig. 3*B* the concentration dependencies of the current amplitude at −150 mV are shown. Here the current amplitudes were normalized to those recorded without Na^+. From these curves apparent dissociation constants for external Na^+ were calculated for the mutant channels: 6.7 mM for the T256Q channel and 11.3 mM for the T256E channel.

In Fig. 4 tail current recordings were performed to further investigate the effect of external Na^+. The voltage protocol is shown in Fig. 4*A*. The membrane potential was stepped to −150 mV for 500 ms, and then it was stepped to different potentials for successively shorter duration as the membrane potential was hyperpolarized. This command significantly reduced possible contamination with the endogenous Cl^- current at very negative potentials. Fig. 4*B* shows the instantaneous current-voltage curves measured at the beginning of the tail potentials. In the absence of external Na^+, these curves represent open-channel properties of KAT1 channels. Slight inward-rectification through the open channel was observed for the WT and T256Q channels. On the other hand, a shallow sigmoidal shape in the instantaneous *I-V* curves for the T256E mutant was observed. Thus, a neutral mutation from T to Q did not change the shape of the *I-V* curves, while an addition of a negative charge (from Q to E) altered the shape of the *I-V* curves from weakly inward rectifying to a sigmoidal shape.

All the instantaneous current-voltage curves for the WT channel are superimposed for the different Na^+ concentrations. The WT channel was little affected by external Na^+ up to 80 mM. On the other hand, the instantaneous current-voltage curves for the mutant channels exhibited distinct features. The current of the T256Q mutant was depressed in a voltage-dependent manner. The depression of the current was augmented at the hyperpolarized potentials. Here, the curves crossed near the equilibrium potential of K^+. The current amplitude for the T256E mutant was depressed over the whole voltage range tested. The curves also crossed at the reversal potential of −30 mV and did not change with Na^+ concentrations. From the shift of the reversal potential for different Na^+ concentrations the permeability ratio, P_{Na}/P_K, was calculated. The P_{Na}/P_K was 0.02 for WT, 0.04 for T256Q and 0.03 for T256E. These results indicate that the K^+ current was depressed with little effect on the selectivity.

Na^+ Blocking Mechanism

In Fig. 5 the Na^+ blocking ratios as a function of the membrane potentials for the mutant channels are shown. The Na^+ blocking is represented by the normalized unblocked ratios, in which the instantaneous current amplitude at each membrane potential for different Na^+ concentrations was divided by that of the corresponding control current amplitude in Na^+-free solution. The voltage-unblocked ratio curves for T256Q exhibited a typical voltage-dependency and its shifts for different concentrations of the blocker. As the Na^+ concentration increased the blocking became apparent and the curves were shifted towards depolarized potentials. These curves were fitted by the two-state Boltzmann function (*see* Materials and Methods). The electric distance thus evaluated was 1.2, indicating deep penetration of Na^+ ion into the pore. Note that these curves were obtained from

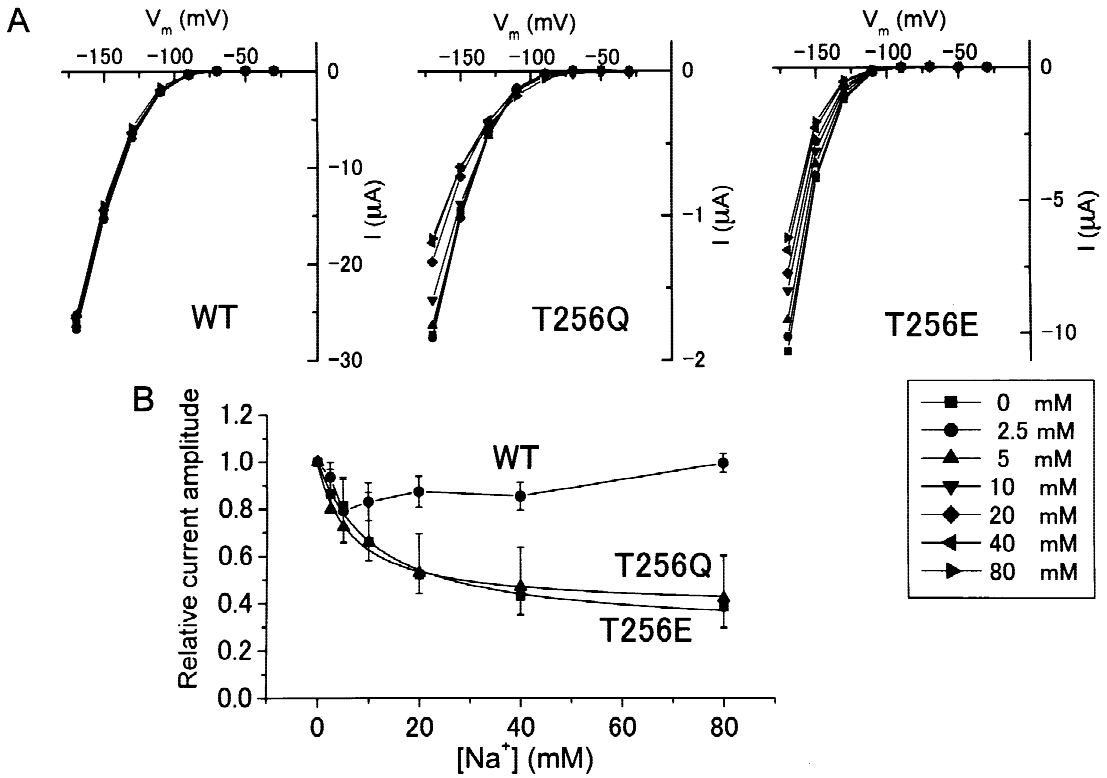

Fig. 3. Dependency of inward KAT1 currents on external Na^+ concentrations. (*A*) The current-voltage curves for different concentrations of external Na^+ ($[Na^+]_o$). The current amplitudes measured at the end of the pulses are plotted as a function of the command voltages. (*B*) Concentration dependency of the current amplitude at −150 mV. The apparent dissociation constant (K_d) was 6.7 mM for T256Q and 11.3 mM for T256E. Current amplitudes for Na^+-containing solutions were normalized by the current amplitudes for the control solution without Na^+.

the instantaneous currents; thus, it is strongly suggested that this inhibition is a fast open-channel blocking.

In contrast, the unblocked ratio of the T256E channel exhibited overall reduction in the whole voltage range tested, including those of the outward currents (Fig. 5*B*). As the concentration increased the current depression became predominant at the negative potentials. When the concentration of external Na^+ was increased, the unblocked ratio curve shifted towards the depolarizing direction and the depressed amplitude recovered significantly at the extreme negative potentials, giving the curve a minimum (the maximum blocking) at around −150 mV. The minimum shifted towards depolarized potentials as the Na^+ concentration was increased. Thus, the effects of external Na^+ on the T256E mutant were three-fold: (i) voltage-independent blocking that saturates at relatively low Na^+ concentration, leaving a rather large fraction of the current. (ii) As the concentration increased the blocking became voltage-dependent. (iii) Further increase in the concentration altered the shape of the curve with a recovery of the unblocked ratio at very negative potentials. The latter phenomenon strongly suggests a release of the blocked Na^+ ion into the cytosol.

To represent these three phases the two-state and three-state Boltzmann functions failed to fit the curves and a more complicated model was necessary. The four-state model, in which the states corresponded to the open, voltage-independent blocking, voltage-dependent blocking and released states, could adequately represent the experimental data. Among the fitted parameters shown in the legend of Fig. 5, the free energy levels of the blocking sites for both mutant channels suggested unstable binding of the blocking Na^+.

Discussion

In this study we investigated the effect of the neutral (T256Q) and the charged (T256E) mutation introduced at the center of the P-region of the KAT1 channel using electrophysiological techniques. The effects of these mutations were three-fold: (i) The activation gating was shifted along the voltage axis with little effect on the gating charge. (ii) The open-channel *I-V* curve changed its shape from weakly inward-rectifying to shallow sigmoidal by the charged mutation from Q to E. (iii) Both mutations induced Na^+-blocking to an otherwise Na^+-insensitive KAT1 channel.

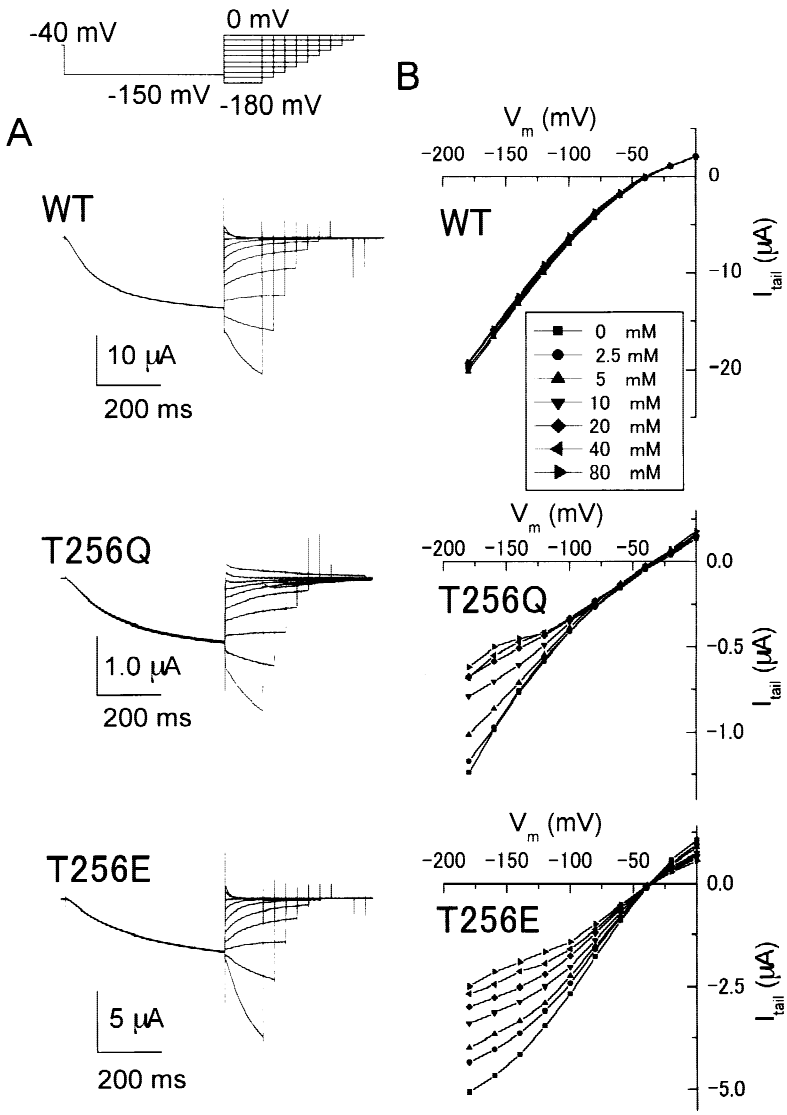

Fig. 4. Tail current recordings and instantaneous current-voltage curves for varying Na^+ concentrations. (*A*) Representative current traces under the "tail" current command for the WT and the mutant T256Q and T256E channels. (*Inset*) The voltage command. The channels were activated at −150 mV for 500 msec and then stepped to various membrane potentials from 0 mV to −200 mV for different durations. (B) The instantaneous current-voltage curves for different Na^+ concentrations. The "instantaneous" current was measured at 1 msec upon the voltage steps to various tail potentials. Na^+ concentration was varied from 0 to 80 mM.

Here, we focus on the mechanism of the Na^+ blocking. Electrophysiological experiments revealed that the mutations diminished the ability of the KAT1 potassium channel to exclude Na^+ from entering the pore. For the T256Q mutant the depressed entrance barrier permitted the external Na^+ to penetrate deeply into the pore. On the other hand, the T256E mutant generated a Na^+ binding site at the entrance of the pore, which induced the reduction of the current amplitude regardless of the current direction. Moreover, at higher concentration of external Na^+, Na^+ penetrates into the pore and eventually gets released to the cytosolic side. Qualitative features of these modifications on the energy profile for Na^+ are schematically shown in Fig. 6*A*.

These functional alterations for permeating K^+ and blocking Na^+ should be interpreted on the structural basis. Here, we refer to the canonical structure of the KcsA channel (Doyle et al., 1998). Closer examination of the crystal structure of the KcsA channel revealed that the corresponding site of T256 is located at the C-terminal end of the pore helix, although the side chain was not resolved in the atomic coordinates. The T256 site is never exposed to the permeation pathway: it is exposed neither to the cavity nor to the selectivity filter. Our experimental results, thus, can not be explained by direct contact of the mutated side chain with permeating ions. Therefore, the altered shape of the open-channel *I-V* curves for K^+ permeation by introducing the charged residue at the pore helix can be interpreted as indicating that the potential profile of permeating K^+ was modified electrostatically through the wall of the selectivity filter.

The entrance barrier for Na^+ was dramatically depressed by the T256 mutations of either Gln or Glu, which is located far from the outer entrance of the pore. Thus, such remote effect of the mutations must be interpreted as an allosteric effect. Recently, systematic stud-

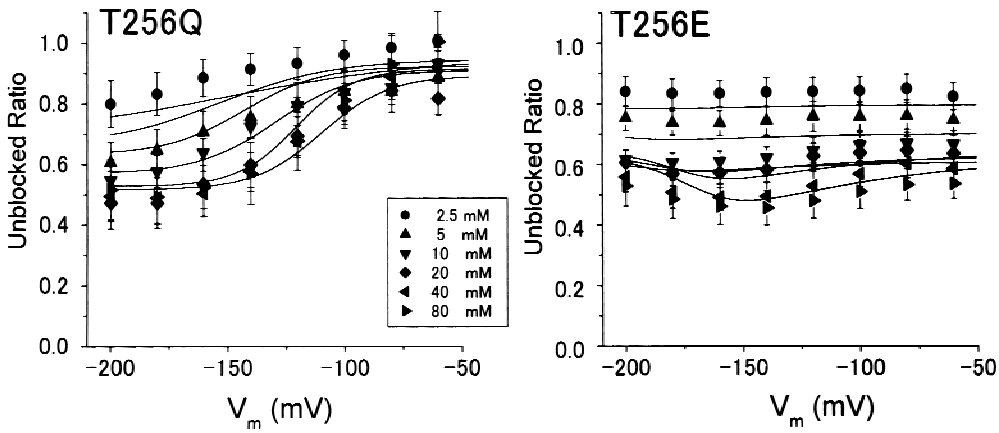

Fig. 5. The concentration and voltage-dependency of the unblocked ratio. The unblocked ratio was calculated from the instantaneous current-voltage curves. For the T256Q mutant the double Boltzmann function was used for the fitting. For the blocking site the ΔG value was 10.6 ± 0.5 *RT*, the electrical distance (δ_1) was 1.2 ± 0.2 and the *C* value was 0.48 ± 0.2. For the T256E mutant a voltage-independent binding site, a voltage-dependent blocking site and release of the blocking was included to represent the unblocking curves. The K_d was 11.3 ± 0.3 mM and *C* was 0.51 ± 0.02 for the voltage-independent binding site. For the blocking site the ΔG_1 value was 11.2 ± 0.4 *RT* and the electrical distance (δ_1) was 1.1 ± 0.1. The ΔG_2 value was 14.0 ± 0.3 *RT* and the δ_2 value was 1.7 ± 0.2.

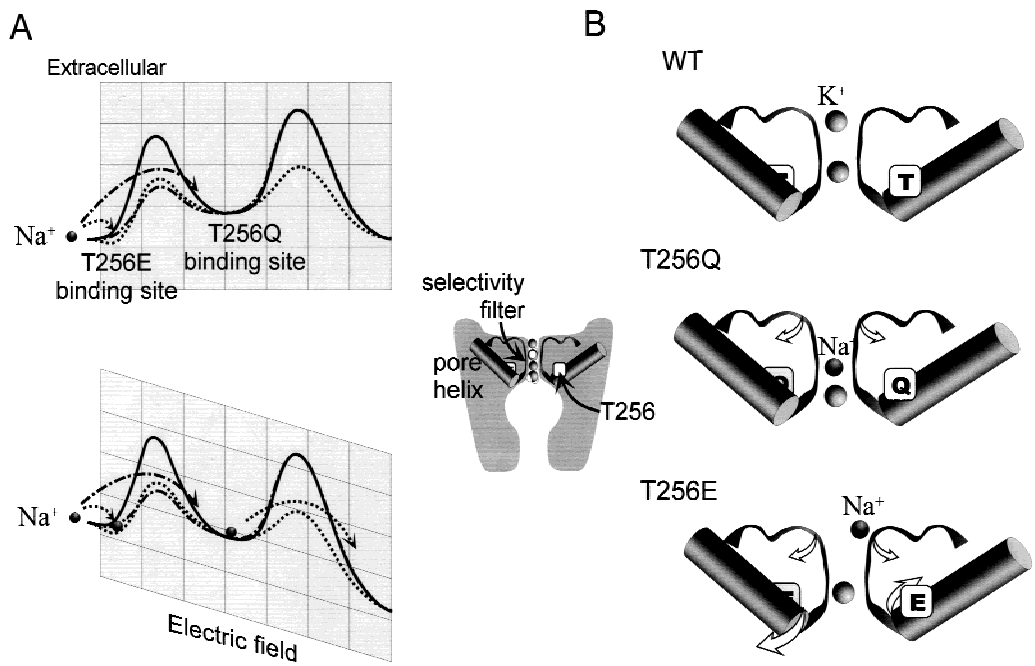

Fig. 6. A hypothetical model of the KAT1 pore for the T256 mutation. (*A*) The potential energy profile for Na^+ blocking deduced from the Boltzmann model. In the WT channel (solid line) the entrance barrier is high enough to completely exclude external Na^+ not only at 0 mV (the upper scheme) but also at negative membrane potentials (the lower scheme). For the T256Q mutant the depressed entrance barrier (dashed-and-dotted line) is still high enough to exclude external Na^+ from the pore in the absence of the membrane potential. In the T256E mutant channel (dotted line) a shallow dip appears near the entrance so that the blocking Na^+ fluctuates rapidly between the dip and the bulk solution. When the negative membrane potential is applied, the entrance barrier for the T256Q mutant is further depressed and external Na^+ is allowed to penetrate deep in the pore. The blocking Na^+ rapidly exits the pore towards the external solution since the internal barrier is still high enough to surmount for blocking Na^+, making the blocking in a fast mode. In the T256E mutant, Na^+ can go over the entrance barrier and stays at the binding site. More hyperpolarization drives the Na^+ permeating through the entire pore. (B) A geometrical interpretation deduced from the potential profiles. A plausible location of the T256 residue corresponding to the homologous site of the KcsA channel is schematically shown on the pore helix, where the silhouette of the KcsA channel is superimposed. The arrows indicate possible displacement of the selectivity filter induced by the perturbation of the core structure. Thus, a wide-open entrance allows blocking Na^+ to penetrate into the pore. The movement of the pore helix would widen the exit barrier of the selectivity filter for T256E that allows the passage of the blocking Na^+ through the pore.

ies were done for Kv channels showing that steric perturbations introduced into the core of the channel proteins altered the stability of the channel proteins and thus altered the gating properties (Li-Smerin, Hackos & Swartz, 2000; Hong & Miller, 2000). Moreover, the structural rearrangement of the helical architecture upon gating was examined using EPR spectroscopy (Perozo, Cortes & Cuello, 1998, 1999; Gross et al., 1999). In KcsA channel, rigid-body motions of the inner helices were accompanied by the movements of the pore helices.

We conclude by proposing a hypothetical model for T256 mutation (Fig. 6*B*) based on the above information on the dynamic structure of potassium channels. Since the T256 site is located in the core of the channel protein, any mutation perturbs the stability of the channel protein, thus shifting the gating curves. Furthermore, the small perturbation introduced into the moving pore-helices brought about rearrangements of the selectivity filter such that the entrance of the pore and the end of the pore open wider, losing the ability to exclude Na^+ (T256Q) and allowing the passage of Na^+ (T256E).

The authors thank Dr. A.F. James (King's College London, London, UK) for critical reading of the manuscript. This work was supported by a Grant-in-Aid from the Ministry of Education, Science and Culture of Japan (12019227, 12206042 and 11660082). This research has been partly supported by CREST of JST (Japan Science and Technology).

References

Anderson, J.A., Huprikar, S.S., Kochian, L.V., Lucas, W.J., Gaber, R.F. 1992. Functional expression of a probable *Arabidopsis thaliana* potassium channel in *Saccharomyces cerevisiae. Proc. Natl. Acad. Sci. USA* **89:**3736–3740

Doyle, D.A., Morais Cabral, J., Pfuetzner, R.A., Kuo, A., Gulbis, J.M., Cohen, S.L., Chait, B.T., MacKinnon, R. 1998. The structure of the potassium channel: molecular basis of K^+ conduction and selectivity. *Science* **280:**69–77

Dreyer, I., Becker, D., Bregante, M., Gambale, F., Lehnen, M., Palme, K., Hedrich, R. 1998. Single mutations strongly alter the K^+-selective pore of the K(in) channel KAT1. *FEBS Lett.* **430:**370–376

Gross, A., Columbus, L., Hideg, K., Altenbach, C., Hubbell, W.L. 1999. Structure of the KcsA potassium channel from *Streptomyces lividans:* site-directed spin labeling study of the second transmembrane segment. *Biochemistry* **38:**10324–10335

Hong, K.H., Miller, C. 2000. The lipid-protein interface of a Shaker (K+) channel. *J. Gen. Physiol.* **115:**51–58

Hoshi, T. 1995. Regulation of voltage dependence of the KAT1 channel by intracellular factors. *J. Gen. Physiol.* **105:**309–328

Ichida, A.M., Schroeder, J.I. 1996. Increased resistance to extracellular cation block by mutation of the pore domain of the *Arabidopsis* inward-rectifying K^+ channel KAT1. *J. Membrane Biol.* **151:**53–62

Kameyama, M., Kakei, M., Sato, R., Shibasaki, T., Matsuda, H., Irisawa, H. 1984. Intracellular Na^+ activated a K^+ channel in mammalian cardiac cells. *Nature* **309:**354–356

Kingsbury, R.W., Epstein, E. 1986. Salt sensitivity in wheat. A case for specific ion toxicity. *Plant Physiol.* **80:**651–654

Lacombe, B., Thibaud, J.B. 1998. Evidence for a multi-ion pore behavior in the plant potassium channel KAT1. *J. Membrane Biol.* **166:**91–100

Li-Smerin, Y., Hackos, D.H., Swartz, K.J. 2000. Alpha-helical structural elements within the voltage-sensing domains of a K^+ channel. *J. Gen. Physiol.* **115:**33–50

Moroni, A.S., Gazzarini, S., Cerana, R., Colombo, R., Sutter, J.U., DiFrancesco, D., Gradmann, D., Thiel, G. 2000. Mutation in pore domain uncovers cation- and voltage-sensitive recovery from inactivation in KAT1 channel. *Biophys. J.* **78:**1862–1871

Perozo, E., Cortes, D.M., Cuello, L.G. 1998. Three-dimensional architecture and gating mechanism of a K^+ channel studied by EPR spectroscopy. *Nat. Struct. Biol.* **5:**459–469

Perozo, E., Cortes, D.M., Cuello, L.G. 1999. Structural rearrangements underlying K^+ channel activation gating. *Science* **285:**73–78

Sabirov, R.Z., Tominaga, T., Miwa, A., Okada, Y., Oiki, S. 1997. A conserved arginine residue in the pore region of an inward rectifier K channel (IRK1) as an external barrier for cationic blockers. *J. Gen. Physiol.* **110:**665–677

Schachtman, D.P., Schroeder, J.I., Lucas, W.J., Anderson, J.A., Gaber, R.F. 1992. Expression of an inward-rectifying potassium channel by the *Arabidopsis* KAT1 cDNA. *Science* **258:**1654–1658

Schroeder, J.I., Ward, J.M., Gassmann, W. 1994. Perspectives on the physiology and structure of inward-rectifying K^+ channels in higher plants: biophysical implications for K+ uptake. *Annu. Rev. Biophys. Biomol. Struct.* **23:**441–471

Uozumi, N., Gassmann, W., Cao, Y., Schroeder, J.I. 1995. Identification of strong modifications in cation selectivity in an *Arabidopsis* inward rectifying potassium channel by mutant selection in yeast. *J. Biol. Chem.* **270:**24276–24281

Uozumi, N., Nakamura, T., Schroeder, J.I., Muto, S. 1998. Determination of transmembrane topology of an inward-rectifying potassium channel from *Arabidopsis thaliana* based on functional expression in *Escherichia coli. Proc. Natl. Acad. Sci. U.S.A.* **95:**9773–9778